

# Isotropization far from equilibrium

Jürgen Berges\*, Szabolcs Borsányi†, Christof Wetterich‡

Universität Heidelberg, Institut für Theoretische Physik  
Philosophenweg 16, 69120 Heidelberg, Germany

## Abstract

Isotropization occurs on time scales much shorter than the thermal equilibration time. This is a crucial ingredient for the understanding of collision experiments of heavy nuclei or other nonequilibrium phenomena in complex many body systems. We discuss in detail the limitations of estimates based on standard “linear” or relaxation-time approximations, where isotropization and thermal equilibration rates agree. For a weak-coupling  $\phi^4$ -model the relaxation-time approximation underestimates the thermal equilibration time by orders of magnitude, in contrast to the isotropization time. The characteristic nonequilibrium isotropization rate can be enhanced as compared to the close-to-equilibrium value. Our results are obtained from the two-particle irreducible effective action, which includes off-shell and memory effects and does not involve a gradient expansion. This allows us to determine the range of validity of a description to lowest-order in gradients, which is typically employed in kinetic equations.

---

\*email: j.berges@thphys.uni-heidelberg.de

†email: s.borsanyi@thphys.uni-heidelberg.de

‡email: c.wetterich@thphys.uni-heidelberg.de

# 1 Introduction and overview

Understanding the dynamics of quantum fields far away from the ground state or thermal equilibrium is a challenge touching many aspects of physics, ranging from early cosmology or collision experiments with heavy nuclei to ultracold quantum gases in the laboratory. One of the most crucial aspects concerns the characteristic time scales on which thermal equilibrium is approached. Much of the recent interest derives from observations in collision experiments of heavy nuclei at RHIC. The experiments seem to indicate the early validity of hydrodynamics, whereas the present theoretical understanding of QCD suggests a longer thermal equilibration time.

However, different quantities effectively thermalize on different time scales and a complete thermalization of all quantities may not be necessary to explain the observations. We have pointed out in Ref. [1] that the prethermalization of crucial observables may occur on time scales dramatically shorter than the thermal equilibration time. In particular, an approximately thermal equation of state may be reached after an extremely short time. From this early time on the effective kinetic temperature is already very close to the final equilibrium value of the temperature and the equilibrium relations between average pressure, energy density and temperature hold. Beyond the (average) equation of state, a crucial ingredient for the applicability of hydrodynamics for collision experiments [2] is the approximate isotropy of the local pressure. More precisely, the diagonal (space-like) components of the local energy-momentum tensor have to be approximately equal. Of particular importance is the possible isotropization far from equilibrium. The relevant time scale for the early validity of hydrodynamics could then be set by the isotropization time [1, 3].

We argue in this paper that isotropization generically happens on time scales much shorter than the thermal equilibration time.<sup>1</sup> For this we concentrate on a general framework for the description of isotropization in far-from-equilibrium quantum field theory [7]. Already for a simple scalar theory with small quartic self-interaction we find that there is a large separation of times between isotropization and thermalization. We compare our results with the most common estimates, which evaluate a

---

<sup>1</sup>A possible mechanism for fast isotropization in QCD in terms of plasma instabilities in high-temperature gauge theories has been proposed in Ref. [3]. We do not consider the interesting topic of plasma instabilities here. For discussions of instabilities in a QCD plasma see Refs. [4, 5]. Other approaches to address fast thermalization include Refs. [6].

relaxation time for small excitations away from equilibrium. This so-called “linear” or relaxation-time approximation [8] assumes that there is a more or less universal characteristic rate for many out-of-equilibrium properties. In particular, in the relaxation-time approximation the characteristic rates for isotropization and thermalization agree. In contrast, we find that for rather general initial conditions the relaxation-time ansatz fails even to give a correct order-of-magnitude estimate of the thermalization time  $\tau_{\text{eq}}$  on which the Bose-Einstein distribution is reached. However, it describes well the (on-shell) isotropization rate,  $\tau_{\text{iso}}^{-1}$ , close to equilibrium at sufficiently late times. For earlier times, we find that the characteristic nonequilibrium isotropization rate can exceed the close-to-equilibrium rate for large initial anisotropies. We go beyond the relaxation-time approximation by calculating the nonequilibrium dynamics from the two-particle irreducible (2PI) effective action to three-loop order which includes scattering, off-shell and memory effects. The nonequilibrium evolution is solved numerically without further assumptions. In particular, we do not apply a gradient expansion. This allows us to determine the range of validity of a description to lowest-order in gradients, which is typically employed in kinetic equations and to motivate the relaxation-time ansatz close to equilibrium. The earliest time for the applicability of the lowest-order gradient expansion is found to be of the order of the characteristic isotropization time  $\tau_{\text{iso}}$ .

We consider a class of anisotropic initial conditions with a high occupation number of modes moving in a narrow momentum range around the “beam direction”  $p_3 = \pm p_{\text{ts}}$ , reminiscent of some aspects of colliding wave packets in the central collision region (cf. Sec. 2). We compute the nonequilibrium isotropization rate for a rather weak coupling of the  $g^2\phi^4$ -interaction. (For our figures we use  $g = 1/2$  and units in terms of the renormalized thermal mass  $m_R$ .) In Fig. 1 we compare this rate with the relaxation-time approximation and with the thermal equilibration time. The lower curve of the figure shows the characteristic nonequilibrium isotropization rate for the momentum  $p_{\text{ts}}$  as a function of time. For times  $t \gtrsim 500/m_R$  the isotropization rate is well described by the standard relaxation-time approximation, i.e. by  $\tau_{\text{iso}}^{-1} = -\Sigma_{\ell}^{(\text{eq})}/2\omega^{(\text{eq})}$ , where the imaginary part of the self-energy  $-\Sigma_{\ell}^{(\text{eq})}/2$  is evaluated for on-shell  $\omega^{(\text{eq})}$  for momentum  $p_{\text{ts}}$ . The thermal equilibrium value  $-\Sigma_{\ell}^{(\text{eq})}/2\omega^{(\text{eq})}$  is indicated by the full square in Fig. 1. At early times, one observes that the relaxation-time rate can underestimate the characteristic nonequilibrium isotropization rate.

For comparison, the upper curve of Fig. 1 shows the nonequilibrium

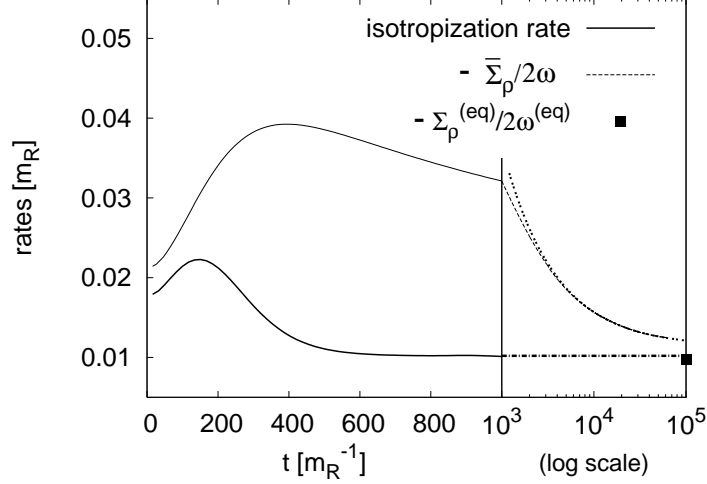


Figure 1: Isotropization and thermalization. The lower curve shows the characteristic nonequilibrium rate for isotropization as a function of time  $t$  in units of the renormalized thermal mass  $m_R$ . At late times it is well approximated by the thermal equilibrium on-shell ratio  $\tau_{\text{iso}}^{-1} = -\Sigma_\rho^{(\text{eq})}/2\omega^{(\text{eq})}$  indicated by the square symbol. This verifies standard relaxation-time approximations for isotropization at sufficiently late times. In contrast to isotropization, the approach to thermal equilibrium is not well described by the relaxation-time approximation. As an example, the upper curve shows  $-\bar{\Sigma}_\rho(t; \omega, \vec{p}_{\text{ts}})/2\omega$ , which characterizes the nonequilibrium evolution of the imaginary-part of the on-shell self-energy. Only at very late times,  $t \gg \tau_{\text{iso}} \simeq 100/m_R$ , it comes rather close to its thermal value. The dotted-line represents a late-time fit explained in Sec. 5.

evolution of the imaginary-part of the self-energy or, more precisely, the on-shell ratio  $-\bar{\Sigma}_\rho(t; \omega, p_{\text{ts}})/2\omega$  (cf. Sec. 2). Only at very late times this rate comes rather close to its thermal equilibrium value  $-\Sigma_\rho^{(\text{eq})}/2\omega^{(\text{eq})}$ . This reflects the slow approach of the momentum distribution to the Bose-Einstein distribution, which will be discussed in Sec. 5. One observes that thermalization is an extremely slow process, and to verify a closer approach in an actual numerical calculation would require to go far beyond the times shown in the figure. Our results clearly demonstrate that the relaxation-time rate  $-\Sigma_\rho^{(\text{eq})}/2\omega^{(\text{eq})}$  cannot be used at all to estimate the correct thermalization time. Most importantly, they show that isotropization happens on time scales much shorter than the thermalization time. This is analysed in detail in this paper.

The paper is organized as follows. In Sec. 2 we derive the nonequilibrium evolution equations from the 2PI effective action and discuss the class of anisotropic initial conditions used in the present work. We solve the approximation of a three-loop 2PI effective action numerically, without further approximations. For further analytical discussion, we consider in Secs. 3 and 4 the linearized dynamics for small deviations from thermal equilibrium. For this we perform a gradient expansion to lowest order and establish its range of applicability by comparing to the “full” result including all orders of derivatives in Sec. 3. This is employed to derive the standard relaxation-time approximation in Sec. 4. The discussion of the numerical results is presented in Sec. 5 and we end with conclusions in Sec. 6.

## 2 Nonequilibrium evolution equations

Consider the single particle excitation which is obtained by adding a particle with momentum  $\vec{p}$  to a system initially in equilibrium. For a weakly interacting system, which has long-lived single-particle excitations, this situation may be described in terms of a Boltzmann equation for the distribution function  $N_p(t)$  for quasi-particles with momentum  $\vec{p}$  and energy  $\omega_p(t)$ .<sup>2</sup> For a small perturbation around thermal equilibrium  $\delta N_p(t) = N_p(t) - N_p^{(\text{eq})}$  the relaxation-time approximation yields [8, 9]

$$\delta N_p(t) = \delta N_p(0) e^{-\gamma(\vec{p})t}, \quad (2.1)$$

with the damping rate  $\gamma(\vec{p})$  determined by the imaginary part of the thermal equilibrium self-energy,  $-\Sigma_e^{(\text{eq})}/2$ , and equilibrium on-shell frequency  $\omega_p^{(\text{eq})}$  according to

$$\gamma(\vec{p}) = -\frac{\Sigma_e^{(\text{eq})}(\omega_p^{(\text{eq})}, \vec{p})}{2\omega_p^{(\text{eq})}}. \quad (2.2)$$

This standard relaxation-time ansatz is widely applied to approximately describe the linearized dynamics around thermal equilibrium.

The question about the range of applicability of the relaxation-time approximation has to be addressed in nonequilibrium quantum field theory. There are various assumptions leading to the above interpretation of the thermal equilibrium quantity (2.2). In order to verify them we have to go

---

<sup>2</sup>Without loss of generality for the argument we employ here spatially homogeneous ensembles.

beyond the standard gradient expansion employed in kinetic descriptions. In addition, no quasi-particle assumption should be employed a priori. We will therefore have to solve the nonequilibrium time evolution including off-shell and memory effects.

## 2.1 2PI effective action and initial conditions

Systematic approximations to describe far-from-equilibrium dynamics as well as thermalization [10, 11, 12, 13, 14, 15, 16, 1, 17] from first principles can be efficiently based on the two-particle irreducible (2PI) effective action [18]:

$$\Gamma[\phi, G] = S_{\text{cl}}[\phi] + \frac{i}{2} \text{Tr} \ln G^{-1} + \frac{i}{2} \text{Tr} G_0^{-1}(\phi) G + \Gamma_2[\phi, G]. \quad (2.3)$$

To  $\Gamma_2[\phi, G]$  only two-particle irreducible diagrams contribute, i.e. diagrams which do not become disconnected by opening two lines. To be specific, we consider a scalar quantum field theory with classical action

$$S_{\text{cl}}[\phi] = \int_x \left( \frac{1}{2} \partial^\mu \phi(x) \partial_\mu \phi(x) - \frac{m^2}{2} \phi^2(x) - g^2 \phi^4(x) \right) \quad (2.4)$$

in the symmetric phase with vanishing field expectation value, i.e.  $\phi = 0$ . The classical inverse propagator is  $iG_0^{-1}(x, y) = \delta^2 S_{\text{cl}}[\phi] / \delta \phi(x) \delta \phi(y)|_{\phi=0}$ . Summation over repeated indices is implied and we use the shorthand notation  $\int_x \equiv \int_{\mathcal{C}} dx^0 \int d^3x$  with  $x \equiv (x^0, \vec{x})$  and  $\mathcal{C}$  denoting a closed time path along the real axis starting at the initial time  $t = 0$ .

The equation of motion for  $G$  is given by the stationarity condition  $\delta \Gamma / \delta G = 0$ , which from Eq. (2.3) reads [18]

$$G^{-1}(x, y) = G_0^{-1}(x, y) - \Sigma(x, y; G). \quad (2.5)$$

The self-energy  $\Sigma$  is related to  $\Gamma_2[G] \equiv \Gamma_2[\phi = 0, G]$  as

$$\Sigma(x, y; G) = 2i \frac{\delta \Gamma_2[G]}{\delta G(x, y)}. \quad (2.6)$$

In order to make the real and imaginary parts explicit we use the decomposition identity [11, 10]

$$G(x, y) = F(x, y) - \frac{i}{2} \rho(x, y) \text{sgn}_{\mathcal{C}}(x^0 - y^0), \quad (2.7)$$

where  $F(x, y)$  denotes the statistical two-point function and  $\rho(x, y)$  the spectral function. The spectral function encodes the equal-time commutation relations:<sup>3</sup>

$$\rho(x, y)|_{x^0=y^0} = 0 \quad , \quad \partial_{x^0}\rho(x, y)|_{x^0=y^0} = \delta(\vec{x} - \vec{y}) . \quad (2.8)$$

To obtain a similar decomposition for the self-energy, we separate  $\Sigma$  in a “local” and “nonlocal” part according to

$$\Sigma(x, y; G) = -i\Sigma^{(0)}(x; G)\delta(x - y) + \Sigma^{(\text{nl})}(x, y; G) . \quad (2.9)$$

Since  $\Sigma^{(0)}$  just corresponds to a space-time dependent mass-shift it is convenient for the following to introduce the notation

$$M^2(x; G) = m^2 + \Sigma^{(0)}(x; G) . \quad (2.10)$$

The imaginary part of the self-energy,  $-\Sigma_\rho/2$ , is determined by

$$\Sigma^{(\text{nl})}(x, y) = \Sigma_F(x, y) - \frac{i}{2}\Sigma_\rho(x, y) \text{sgn}_C(x^0 - y^0) . \quad (2.11)$$

Nonequilibrium dynamics requires the specification of an initial state. While the corresponding initial conditions for the spectral function are governed by the commutation relations (2.8), the statistical function  $F(x, y)$  and first derivatives at  $x^0 = y^0 = 0$  have to be specified. Here we consider systems described by Gaussian *initial* density matrices. This represents no approximation for the (non-Gaussian) dynamics for times  $t > 0$ , but just constrains the class of initial conditions. We consider a situation with an initially high occupation number of modes moving in a narrow momentum range around the “beam direction”  $p_3 \equiv p_\parallel = \pm p_{\text{ts}}$ . The occupation numbers for modes with momenta perpendicular to this direction,  $p_1^2 + p_2^2 \equiv p_\perp^2$ , are small or vanishing. The situation is reminiscent of some aspects of the anisotropic initial stage in the central region of collision experiments of heavy nuclei.<sup>4</sup> More explicitly, we employ a class of initial conditions parametrized as

$$F(t_1, t_2; \vec{p})|_{t_1=t_2=0} = \frac{n_0(\vec{p}) + 1/2}{\omega_p} , \quad (2.12)$$

---

<sup>3</sup>It is also directly related to the retarded propagator  $\rho(x, y)\Theta(x^0 - y^0)$ , or the advanced one  $-\rho(x, y)\Theta(y^0 - x^0)$ .

<sup>4</sup>Other interesting scenarios include “color-glass”-type initial conditions with distributions  $\sim \exp(-\sqrt{p_\perp^2}/Q_s)$  peaked around  $p_3 = 0$  with “saturation” momentum  $Q_s$ .

with  $\partial_{t_1} F(t_1, 0; \vec{p})|_{t_1=0} = 0$ ,  $\partial_{t_1} \partial_{t_2} F(t_1, t_2; \vec{p})|_{t_1=t_2=0} = [n_0(\vec{p}) + 1/2] \omega_p$  for  $\omega_p \equiv \sqrt{p_\perp^2 + p_\parallel^2 + M_0^2}$  and  $M_0^2 \equiv M^2(t_1 = 0)$ . The initial distribution function  $n_0(\vec{p})$  is peaked around the “tsunami” momentum  $p_{ts}$  with amplitude  $A$  and width  $\sigma$ :

$$n_0(\vec{p}) = A \exp \left\{ -\frac{1}{2\sigma^2} [p_\perp^2 + (|p_\parallel| - p_{ts})^2] \right\}. \quad (2.13)$$

With these initial conditions, for our scalar model the most general statistical two-point function can be written as

$$F(t_1, t_2; \vec{p}) = F(t_1, t_2; p_\perp, p_\parallel), \quad (2.14)$$

and equivalently for the spectral function, as well as for the self-energies  $\Sigma_F(t_1, t_2; \vec{p}) = \Sigma_F(t_1, t_2; p_\perp, p_\parallel)$  and  $\Sigma_\rho(t_1, t_2; \vec{p}) = \Sigma_\rho(t_1, t_2; p_\perp, p_\parallel)$ .

All momentum integrals appearing in this paper will be regularized on a lattice, with the momentum cutoff  $\Lambda$  chosen such that  $\Lambda \gg p_{ts}$ . The renormalization of 2PI effective actions has been discussed in detail in Refs. [21, 19, 22, 23]. For the weak couplings employed here we follow the lines of Ref. [17] to ensure that the relevant length scales are larger than the lattice spacing. We note that quantities such as the renormalized mass or renormalized damping rates can be directly inferred from the oscillation frequency and damping of  $F(t_1, t_2; \vec{p} = 0)$  or  $\rho(t_1, t_2; \vec{p} = 0)$  (see Eq. (5.1) below) [7].

## 2.2 Time-evolution equations

The exact time-evolution equations for known self-energies  $\Sigma_F$  and  $\Sigma_\rho$  are obtained from the stationarity condition of the effective action, or Eq. (2.5) by convolution with  $G$ . Using the decomposition identities (2.7) and (2.11), these are coupled differential equations for the spectral and statistical functions [11, 10]:

$$\begin{aligned} [\partial_{t_1}^2 + \vec{p}^2 + M^2(t_1)] F(t_1, t_2; \vec{p}) &= - \int_0^{t_1} dt' \Sigma_\rho(t_1, t'; \vec{p}) F(t', t_2; \vec{p}) \\ &\quad + \int_0^{t_2} dt' \Sigma_F(t_1, t'; \vec{p}) \rho(t', t_2; \vec{p}), \\ [\partial_{t_1}^2 + \vec{p}^2 + M^2(t_1)] \rho(t_1, t_2; \vec{p}) &= - \int_{t_2}^{t_1} dt' \Sigma_\rho(t_1, t'; \vec{p}) \rho(t', t_2; \vec{p}). \end{aligned} \quad (2.15)$$



They are causal equations with integrals over the time history, starting from the time  $t_0 = 0$  at which the initial conditions of Sec. 2.1 are specified.

A characteristic anisotropy measure can be chosen as

$$\Delta F(t_1, t_2; \bar{q}) \equiv F(t_1, t_2; p_\perp = 0, p_\parallel = \bar{q}) - F(t_1, t_2; p_\perp = \bar{q}, p_\parallel = 0), \quad (2.16)$$

which vanishes for the case of an isotropic correlator. Its exact evolution equation for known self-energies reads according to (2.15):

$$\begin{aligned} & [\partial_{t_1}^2 + \bar{q}^2 + M^2(t_1)] \Delta F(t_1, t_2; \bar{q}) = \\ & - \int_0^{t_1} dt' [\bar{\Sigma}_\rho(t_1, t'; \bar{q}) \Delta F(t', t_2; \bar{q}) + \Delta \Sigma_\rho(t_1, t'; \bar{q}) \bar{F}(t', t_2; \bar{q})] \\ & + \int_0^{t_2} dt' [\bar{\Sigma}_F(t_1, t'; \bar{q}) \Delta \rho(t', t_2; \bar{q}) + \Delta \Sigma_F(t_1, t'; \bar{q}) \bar{\rho}(t', t_2; \bar{q})] . \end{aligned} \quad (2.17)$$

Here we have defined the average

$$\bar{F}(t_1, t_2; \bar{q}) \equiv \frac{1}{2} [F(t_1, t_2; p_\perp = 0, p_\parallel = \bar{q}) + F(t_1, t_2; p_\perp = \bar{q}, p_\parallel = 0)] , \quad (2.18)$$

and equivalently for the corresponding average of the spectral function,  $\bar{\rho}(t_1, t_2; \bar{q})$ , and the corresponding average self-energies  $\bar{\Sigma}_\rho(t_1, t_2; \bar{q})$  and  $\bar{\Sigma}_F(t_1, t_2; \bar{q})$ .

We solve Eq. (2.15) numerically using the coupling- or loop-expansion of the 2PI effective action to order  $g^4$  or three-loop order without further approximations. To this order the effective mass term is

$$M^2(t_1) = m^2 + 12g^2 \int_{\vec{p}} F(t_1, t_1; \vec{p}) \quad (2.19)$$

and the self-energies are [11]

$$\begin{aligned} \Sigma_F(t_1, t_2; \vec{p}) &= -96g^4 \int_{\vec{q}, \vec{k}} F(t_1, t_2; \vec{p} - \vec{q} - \vec{k}) \left[ F(t_1, t_2; \vec{q}) F(t_1, t_2; \vec{k}) \right. \\ &\quad \left. - \frac{3}{4} \rho(t_1, t_2; \vec{q}) \rho(t_1, t_2; \vec{k}) \right], \\ \Sigma_\rho(t_1, t_2; \vec{p}) &= -288g^4 \int_{\vec{q}, \vec{k}} \rho(t_1, t_2; \vec{p} - \vec{q} - \vec{k}) \left[ F(t_1, t_2; \vec{q}) F(t_1, t_2; \vec{k}) \right. \\ &\quad \left. - \frac{1}{12} \rho(t_1, t_2; \vec{q}) \rho(t_1, t_2; \vec{k}) \right], \end{aligned} \quad (2.20)$$

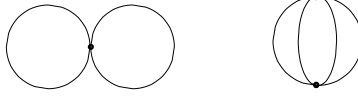


Figure 2: Diagrammatic representation of the contributions to  $\Gamma_2[G]$  to three-loop order.



Figure 3: Diagrammatic representation of the corresponding contributions to the self-energy  $\Sigma$ .

using the notation  $\int_{\vec{p}} \equiv \int d^3p/(2\pi)^3$ . The diagrammatic representation of the approximation is given in Figs. 2 and 3. We solve Eqs. (2.15)–(2.20) for the initial conditions numerically without further approximations along the lines of Refs. [10, 7].

In terms of these quantities the energy density  $\varepsilon \equiv T^{00}$  and pressure components  $P^i \equiv T^{ii}$  ( $i = 1, 2, 3$ ) are given by the diagonal elements of the energy-momentum tensor  $T^{\mu\nu}$  with

$$\begin{aligned} \varepsilon(t_1) = & \frac{1}{2} \int_{\vec{q}} \left[ \partial_{t_1} \partial_{t_2} F(t_1, t_2; \vec{q})|_{t_1=t_2} \right. \\ & + \left( \vec{q}^2 + m^2 + 6g^2 \int_{\vec{p}} F(t_1, t_1; \vec{p}) \right) F(t_1, t_1; \vec{q}) \Big] \\ & - \frac{1}{4} \int_{\vec{q}} \int_0^{t_1} dt' [\Sigma_F(t_1, t'; \vec{q}) \rho(t', t_1; \vec{q}) - \Sigma_\rho(t_1, t'; \vec{q}) F(t', t_1; \vec{q})] , \end{aligned} \quad (2.21)$$

$$\begin{aligned} P^i(t_1) = & \frac{1}{2} \int_{\vec{q}} \left[ \partial_{t_1} \partial_{t_2} F(t_1, t_2; \vec{q})|_{t_1=t_2} + 2q_i^2 F(t_1, t_1; \vec{q}) \right. \\ & - \left( \vec{q}^2 + m^2 + 6g^2 \int_{\vec{p}} F(t_1, t_1; \vec{p}) \right) F(t_1, t_1; \vec{q}) \Big] \\ & + \frac{1}{4} \int_{\vec{q}} \int_0^{t_1} dt' [\Sigma_F(t_1, t'; \vec{q}) \rho(t', t_1; \vec{q}) - \Sigma_\rho(t_1, t'; \vec{q}) F(t', t_1; \vec{q})] . \end{aligned} \quad (2.22)$$

For an efficient (numerical) evaluation of these expressions it is advantageous to replace time integrals by time derivatives of  $F(t_1, t_2; \vec{p})$  using Eq. (2.15).

### 2.3 Thermal equilibrium

We finally note that out of equilibrium  $F$  and  $\rho$  are a priori *not* related by a fluctuation-dissipation relation. In contrast, in thermal equilibrium the periodicity (“KMS”) condition for the propagator,  $G(x, y)|_{x^0=0} = G(x, y)|_{x^0=-i\beta}$ , leads in Fourier space to the relation<sup>5</sup>

$$F^{(\text{eq})}(\omega, \vec{p}) = \left( n_{\text{BE}}(\omega) + \frac{1}{2} \right) \varrho^{(\text{eq})}(\omega, \vec{p}), \quad (2.23)$$

with the Bose-Einstein distribution  $n_{\text{BE}}(\omega) = 1/[\exp(\beta\omega) - 1]$  for inverse temperature  $\beta$ . The equivalent relation holds for the statistical ( $\Sigma_F$ ) and spectral ( $\Sigma_\varrho$ ) part of the self-energy [10]. We emphasize that we solve the nonequilibrium dynamics without any assumption about the validity of a fluctuation-dissipation relation. In order to compare the nonequilibrium late-time results to thermal equilibrium, we calculate in addition the thermal solution. This can be conveniently obtained from the  $\rho$ -part of Eq. (2.15) along the lines of Refs. [19, 15]. The equation for the translation invariant thermal  $\rho^{(\text{eq})}(s, \vec{p})$  with  $s = t - t'$  can be closed using Eq. (2.23) to eliminate  $F^{(\text{eq})}$  with

$$\int ds F^{(\text{eq})}(s; \vec{p}) \cos(\omega s) = \left( n_{\text{BE}}(\omega) + \frac{1}{2} \right) \int ds \rho^{(\text{eq})}(s; \vec{p}) \sin(\omega s). \quad (2.24)$$

## 3 Comparison with lowest-order gradient expansion

For further analytical discussion — not to solve the equations — we consider the exact equations (2.15) in a lowest-order gradient expansion [26, 27, 28, 29, 30, 31, 32, 33, 34, 7] and use it to discuss the dynamics in the vicinity of thermal equilibrium.<sup>6</sup> This will also allow us to recover the relaxation-time approximation employing the corresponding additional assumptions described below in Sec. 4. Since the range of applicability of a gradient expansion is restricted to sufficiently homogeneous correlations at sufficiently late times, one cannot consider the early-time behavior in this case. We emphasize, however, that we are solving the nonequilibrium evolution using Eqs. (2.15), which do not suffer from this restriction. In particular, our

---

<sup>5</sup>In order to have a real  $\varrho^{(\text{eq})}(\omega, \vec{p})$  we employ the Fourier-transformation as in Eq. (3.1) below, which includes an additional factor of  $-i$ .

<sup>6</sup>The following general analysis is not restricted to a coupling- or loop-expansion.

results can then be used to establish whether, and at what time, a gradient expansion can be applied.

For sufficiently late times  $t_1, t_2 \gg t_0$  the quantitative results turn out not to be notably affected by sending  $t_0 \rightarrow -\infty$ , which is required in a gradient expansion for practical purposes. Introducing relative and central coordinates,  $s \equiv t_1 - t_2$  and  $t \equiv (t_1 + t_2)/2$ , the Wigner transformed correlators are

$$\begin{aligned} F(t; \omega, \vec{p}) &= \int ds e^{i\omega s} F(t + s/2, t - s/2; \vec{p}), \\ \varrho(t; \omega; \vec{p}) &= -i \int ds e^{i\omega s} \rho(t + s/2, t - s/2; \vec{p}), \end{aligned} \quad (3.1)$$

where the factor  $i$  is introduced to obtain a real Wigner-space  $\varrho(t; \omega; \vec{p})$ . Note that the time integral over  $s$  is bounded by  $\pm 2t$  because of the initial-value problem with  $t_1, t_2 \geq 0$ . The equivalent transformation is done for the self-energies to obtain  $\Sigma_F(t; \omega, \vec{p})$  and  $\Sigma_\varrho(t; \omega, \vec{p})$ . In lowest-order of the expansion in derivatives of  $t$  and  $\omega$ , i.e. neglecting second derivatives, one finds from the equations (2.15) [24, 25, 26]:

$$\begin{aligned} 2\omega \frac{\partial}{\partial t} F(t; \omega, \vec{p}) &= \Sigma_\varrho(t; \omega, \vec{p}) F(t; \omega, \vec{p}) - \Sigma_F(t; \omega, \vec{p}) \varrho(t; \omega, \vec{p}), \\ 2\omega \frac{\partial}{\partial t} \varrho(t; \omega, \vec{p}) &= 0. \end{aligned} \quad (3.2)$$

We note that the structure of the gradient expanded equations is very similar to the exact equations (2.15). In lowest order of the expansion the evolution equation for the spectral function  $\varrho(t; \omega, \vec{p})$  becomes trivial. A frequently employed variant of the equations (3.2) also takes into account the change of the effective mass  $M^2$  of Eq. (2.19) with respect to  $t$ . This contribution  $\sim (\partial M^2 / \partial t)(\partial F / \partial \omega)$  and the Poisson brackets entering at second order, as well as all higher orders are neglected in the lowest-order expression (3.2) [24, 26].

Following the same lines, in lowest-order of the gradient expansion one finds from Eq. (2.17) the anisotropy equation

$$\begin{aligned} 2\omega \frac{\partial}{\partial t} \Delta F(t; \omega, \vec{q}) &= \bar{\Sigma}_\varrho(t; \omega, \vec{q}) \Delta F(t; \omega, \vec{q}) + \Delta \Sigma_\varrho(t; \omega, \vec{q}) \bar{F}(t; \omega, \vec{q}) \\ &\quad - \bar{\Sigma}_F(t; \omega, \vec{q}) \Delta \varrho(t; \omega, \vec{q}) - \Delta \Sigma_F(t; \omega, \vec{q}) \bar{\varrho}(t; \omega, \vec{q}), \\ 2\omega \frac{\partial}{\partial t} \Delta \varrho(t; \omega, \vec{q}) &= 0. \end{aligned} \quad (3.3)$$

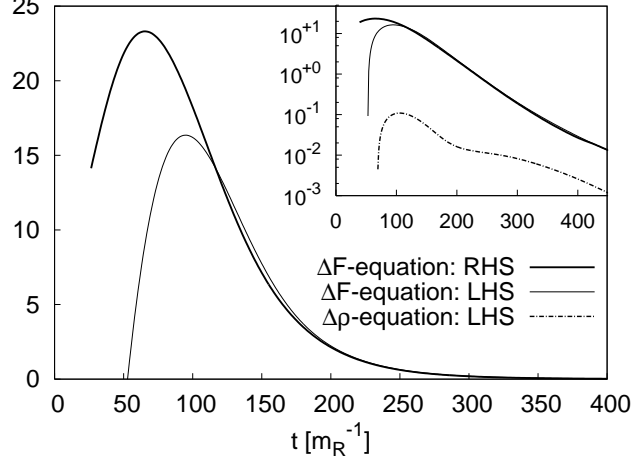


Figure 4: Range of validity of the gradient expansion. The solid line shows the on-shell  $\overline{\Sigma}_\varrho \Delta F + \Delta \Sigma_\varrho \overline{F} - \overline{\Sigma}_F \Delta \varrho - \Delta \Sigma_F \overline{\varrho}$  (thick line) and  $2\omega \frac{\partial}{\partial t} \Delta F$  (thin line) in Wigner coordinates, as computed from the solution of the “full” equation (2.17) without a gradient expansion. If the gradient expansion to lowest order is correct, then both lines have to agree according to the  $\Delta F$ - and  $\Delta \varrho$ -equations (3.3). The inset shows the same results on a logarithmic scale to make the small  $2\omega \frac{\partial}{\partial t} \Delta \varrho$  visible. From these quantities we observe that the lowest-order gradient expansion becomes valid on a time scale similar to the isotropization time  $\tau_{\text{iso}}$ .

In order to establish the range of applicability of the gradient expansion, we compare with the results obtained from Eqs. (2.15)–(2.20) which include *all* orders of gradients: We compute the Wigner-transforms of the results for  $\Delta F(t_1, t_2; \vec{p})$  and  $\Delta \rho(t_1, t_2; \vec{p})$  according to (3.1). From this we then evaluate  $2\omega \frac{\partial}{\partial t} \Delta F$ , and  $\overline{\Sigma}_\varrho \Delta F + \Delta \Sigma_\varrho \overline{F} - \overline{\Sigma}_F \Delta \varrho - \Delta \Sigma_F \overline{\varrho}$ , for on-shell  $\omega$ . The results are represented as separate curves in Fig. 4. If the gradient expansion to lowest order is correct, then both lines have to agree according to Eqs. (3.3), where these contributions appear as the LHS and the RHS of the equations. At early times the agreement is poor and the gradient expansion to lowest order cannot be applied as expected. We recall that because of the initial-value problem with  $t_1, t_2 \geq 0$  the time integral in the Wigner transform (3.1) is finite. However, the effects of the necessarily finite time interval for a nonequilibrium evolution quickly become irrelevant and do not notably affect the curves. For times  $t \gtrsim 100/m_R$  the two curves approach each other closely and the full result is indeed well approximated by the lowest-

order contributions in the derivative expansion. This establishes the use of a gradient expansion for the anisotropy dynamics at sufficiently late times. We note that, in contrast to the differences  $\Delta F$  and  $\Delta \varrho$  measuring the anisotropy, the agreement was found to be much worse for  $F$  and  $\varrho$ . Their description in terms of a lowest-order gradient expansion is very poor for the times displayed here.

## 4 Linear and relaxation-time approximation

Linearized dynamics around thermal equilibrium can provide a valid description at sufficiently late times, when the system is approaching thermal equilibrium. We denote the four-momentum  $p = (\omega, \vec{p})$  and write

$$F(t; p) = F^{(\text{eq})}(p) + \delta F(t; p). \quad (4.1)$$

Equation (3.2) can be linearized in the deviations  $\delta F(t; p)$  from the  $t$ -independent thermal equilibrium value  $F^{(\text{eq})}(p)$ :

$$\begin{aligned} \frac{\partial}{\partial t} \delta F(t; p) &= - \int_q S(p, q) \delta F(t; q) \\ &\equiv - \int_q S'(p, q) \delta F(t; q) + \frac{\Sigma_\varrho^{(\text{eq})}(p)}{2\omega} \delta F(t; p), \end{aligned} \quad (4.2)$$

with  $\int_q \equiv \int d^4 q / (2\pi)^4$ . Here the “stability matrix”  $S(p, q)$  is  $t$ -independent and has to be evaluated in thermal equilibrium. To be explicit we use the self-energies (2.20) in thermal equilibrium for which the matrix  $S'$  in (4.2) reads

$$\begin{aligned} S'(p, q) &= \frac{288g^4}{\omega} \int_k \left\{ \varrho^{(\text{eq})}(p - q - k) F^{(\text{eq})}(k) F^{(\text{eq})}(p) \right. \\ &\quad \left. - \frac{1}{2} \left[ F^{(\text{eq})}(p - q - k) F^{(\text{eq})}(k) + \frac{1}{4} \varrho^{(\text{eq})}(p - q - k) \varrho^{(\text{eq})}(k) \right] \varrho^{(\text{eq})}(p) \right\}, \end{aligned} \quad (4.3)$$

with the equilibrium statistical and spectral function related by Eq. (2.23). We have written the diagonal contribution  $\sim \Sigma_\varrho^{(\text{eq})}$  explicitly in the second line of Eq. (4.2), since the relaxation-time approximation corresponds to assuming  $\int S' \delta F \equiv 0$ . The omission of the “off-diagonal” elements in the matrix  $S'(p, q)$  is a crucial feature of the relaxation-time approximation and

responsible for its failure to describe correctly the large-time dynamics of thermalization as will be discussed below.<sup>7</sup> It corresponds to the picture that the dynamics of a single excitation  $\delta F(t; p)$  can be described independently of the other modes, assuming equilibrium values for all  $F(q)$  except for the mode  $q = p$ . However, the true linear description is given by the full stability matrix  $S(p, q)$ .

Using a language of discrete momenta and a four-volume  $\Omega$ , for very large time the evolution will be dictated by the smallest eigenvalue  $\lambda_{\min}$  of  $S/\Omega$  according to

$$\delta F \sim F_{\min} e^{-\lambda_{\min} t}, \quad (4.4)$$

with  $F_{\min}$  the eigenvector corresponding to  $\lambda_{\min}$ . The thermalization time can be associated with  $\lambda_{\min}^{-1}$ . (We omit here the complications that  $\lambda_{\min}$  may be degenerate or vanish in the infinite volume limit.) The size of  $\lambda_{\min}$  may be much smaller than the size of typical diagonal elements of the stability matrix or  $\Sigma_{\varrho}^{(\text{eq})}/2\omega$ . The latter determines the characteristic time for a given single mode in the relaxation-time approximation according to Eq. (4.7) or (4.10) below. We also note that the eigenvector  $F_{\min}$  is typically not in the direction of the initial small deviation  $\delta F$ . Deviations from thermal equilibrium will be excited for *all* modes during the approach to equilibrium, explaining the possible failure of an approximation based on a single excitation.

In order to compute the eigenvalues of the linearization matrix in Eq. (4.2), one may be tempted to diagonalize the matrix numerically from the regularized expression of the field-theory.<sup>8</sup> However, here we are only interested in the smallest relevant eigenvalue which determines the late-time behavior. In this case, it is more efficient to directly solve the time evolution equations (2.15) along the lines of Ref. [10]. The smallest eigenvalue (or an upper bound for it) can then be obtained from the late-time limit of the dynamics. In the infinite volume limit the smallest eigenvalue may approach zero. The presence of vanishing eigenvalue(s) can invalidate the linear approach even for small perturbations around equilibrium. We emphasize that the direct solution of the time evolution equations (2.15) is not restricted to the linearized dynamics discussed in this section.

---

<sup>7</sup>Cf. also the discussion in Ref. [35].

<sup>8</sup>Note that the matrix is obtained from the gradient expanded equations in the limit of an initial time in the remote past, i.e.  $t_0 \rightarrow -\infty$ . The latter damps out the unstable directions around thermal equilibrium that are present in the reversible dynamics for finite  $t_0$ .

Before turning to the full numerical results in Sec. 5, we consider the dynamics in the relaxation-time approximation. In general, the relaxation-time approximation does not describe the full linearized dynamics since it involves further assumptions. In this approximation one assumes that in the immediate vicinity of thermal equilibrium the dynamics is well approximated by omitting the contributions involving the matrix  $S'$  in Eq. (4.2). We first discuss isotropization. Within the relaxation-time approximation the evolution equation for  $\Delta F$  is given by

$$2\omega \frac{\partial}{\partial t} \Delta F(t; \omega, \bar{q}) \stackrel{\text{relax. time}}{=} \Sigma_{\varrho}^{(\text{eq})}(\omega, \bar{q}) \Delta F(t; \omega, \bar{q}). \quad (4.5)$$

The solution reads

$$\Delta F(t; \omega, \bar{q}) \stackrel{\text{relax. time}}{=} \Delta F_0(\omega, \bar{q}) e^{-\gamma_{\text{iso}}(\omega, \bar{q})t}, \quad (4.6)$$

where the isotropization rate is determined by the imaginary part of the thermal self-energy,  $-\Sigma_{\varrho}^{(\text{eq})}/2$ , according to

$$\gamma_{\text{iso}}(\omega, \bar{q}) \stackrel{\text{relax. time}}{=} -\frac{\Sigma_{\varrho}^{(\text{eq})}(\omega, \bar{q})}{2\omega}. \quad (4.7)$$

We next turn to thermal equilibration. In thermal equilibrium the ratio of the Wigner-transformed statistical and spectral function becomes

$$\frac{F^{(\text{eq})}(\omega, \vec{p})}{\varrho^{(\text{eq})}(\omega, \vec{p})} = n_{\text{BE}}(\omega) + \frac{1}{2} \quad (4.8)$$

according to the fluctuation-dissipation relation (2.23), with the  $\vec{p}$ -independent Bose-Einstein distribution function  $n_{\text{BE}}(\omega)$ . In order to discuss the approach to thermal equilibrium, we consider the behavior of  $F/\varrho$  at late times. In the relaxation-time approximation one finds

$$\frac{F(t; \omega, \vec{p})}{\varrho^{(\text{eq})}(\omega, \vec{p})} \stackrel{\text{relax. time}}{=} n_{\text{BE}}(\omega) + \frac{1}{2} + \left[ \frac{F_0(\omega, \vec{p})}{\varrho^{(\text{eq})}(\omega, \vec{p})} - n_{\text{BE}}(\omega) - \frac{1}{2} \right] e^{-\gamma_{\text{eq}}(\omega, \vec{p})t}. \quad (4.9)$$

Here we have used the fact that in thermal equilibrium  $\Sigma_F^{(\text{eq})}/\Sigma_{\varrho}^{(\text{eq})} = n_{\text{BE}} + \frac{1}{2}$ . This yields the familiar result that the thermalization rate in the relaxation-time approximation is determined by the imaginary part of the thermal self-energy according to

$$\gamma_{\text{eq}}(\omega, \vec{p}) \stackrel{\text{relax. time}}{=} -\frac{\Sigma_{\varrho}^{(\text{eq})}(\omega, \vec{p})}{2\omega}. \quad (4.10)$$



Of course, comparing to Eq. (4.7) one observes the well-known result that the isotropization and thermalization rates agree in the relaxation-time approximation, i.e.  $\gamma_{\text{iso}} = \gamma_{\text{eq}}$  in this case. We emphasize that in general isotropy is a necessary condition for thermal equilibrium while the reverse is not. Below we will show that beyond the relaxation-time approximation  $\Delta F$  can vanish with a characteristic inverse rate, which is very different from the time for the approach of  $F$  to equilibrium.

For sufficiently weak coupling the relaxation-time rate can be computed from perturbation theory, which we denote by  $\gamma^{(\text{pert})}$ . For the zero-momentum mode this is found to be [36]

$$\gamma^{(\text{pert})} = \frac{9g^4 T^2}{2\pi^3 m_R} \text{Li}_2(e^{-m_R/T}) \quad (4.11)$$

where  $\text{Li}_2(z)$  is the second poly-logarithmic function, defined by

$$\text{Li}_2(z) = - \int_0^z dw \frac{\ln(1-w)}{w}. \quad (4.12)$$

In the high-temperature limit this becomes

$$\gamma^{(\text{pert})} = \frac{3g^4 T^2}{4\pi m_R}. \quad (4.13)$$

Our numerical results explained in the next section show that for late times the isotropization rate  $\gamma_{\text{iso}}$  is actually well described (on-shell) by the relaxation-time approximation. In particular, for sufficiently weak coupling the perturbative expressions for the zero-momentum mode provide a rather good estimate for this rate. On the other hand, thermalization occurs for times that exceed by several orders of magnitude the relaxation-time estimate (4.10). Nevertheless, examples in the literature show that for some very specific initial conditions the relaxation-time approximation can give a rather good estimate for the thermal equilibration rate as well (cf., in particular, Refs. [20, 15]).

One may therefore ask what are the conditions for the relaxation-time approximation to hold. First, one has to distinguish between quantities whose vanishing corresponds to an enhanced symmetry from more generic quantities. Once an ensemble is isotropic it always remains so at late times. The vanishing of  $\Delta F$  obviously corresponds to an enhanced symmetry, i.e. rotation symmetry. The isotropic states may be considered as a submanifold

of all states: Isotropization describes then the time evolution for excitations orthogonal to this submanifold. The relevant piece in the stability matrix  $S$  concerns the non-singlet representations of the rotation group. One concludes that isotropization is determined by the smallest eigenvalue in this submatrix rather than the smallest eigenvalue of  $S$ . (The stability matrix is block diagonal in the different irreducible representations of the rotation group.) Eigenvalues relevant for isotropization may all be much larger than the smallest eigenvalue  $\lambda_{\min}$ , which typically occurs in the singlet sector, such that the isotropization time is indeed much shorter than the thermalization time. After the system has become isotropic there still remains a slow flow within the isotropic subspace towards the equilibrium point.

We next ask under what circumstances the relaxation-time approximation can be used to describe thermalization. Let us start with a specific initial condition where only one mode is excited infinitesimally. In general, due to the off-diagonal elements in the stability matrix  $S$  the other modes will be excited as well in the course of the linear evolution. This defines a characteristic time scale where these other modes reach amplitudes of the same order of magnitude as the initially perturbed mode. The relaxation-time approximation typically becomes invalid for larger times. On the other hand, for practical purposes the deviation from equilibrium may be already substantially reduced at that time and the following evolution of not much relevance. In this case the relaxation-time approximation can be used in practice. It has been actually observed in Refs. [20, 15] that the relaxation-time approximation provides a rather good description for a single initially excited mode of finite amplitude, with all other modes in equilibrium. Since the off-diagonal elements of  $S'$  involve a volume factor  $\Omega^{-1}$  from the  $q$ -integration in Eq. (4.2), the relaxation-time approximation becomes valid in the infinite volume limit if a set of modes of measure zero is initially excited. However, realistic initial conditions involve some distribution of initially excited modes (for example a Gaussian). Then the sum over the initial modes in Eq. (4.2) compensates, at least partially, the volume factor. For our initial conditions described in Sec. 2.1, even though chosen quite narrow in momentum space, we find that the relaxation-time approximation fails to describe the approach to thermal equilibrium. We believe that this failure happens for a very wide class of generic initial conditions.

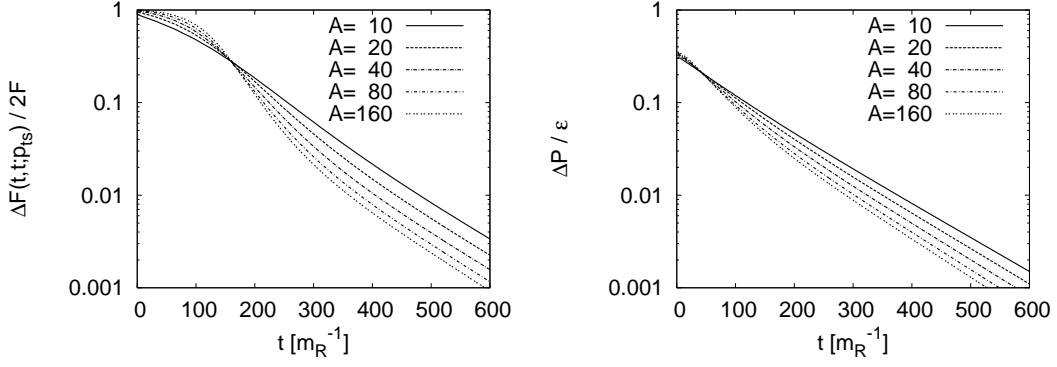


Figure 5: Isotropization. On the left the normalized anisotropy correlator  $\Delta F(t, t; p_{ts})$  is shown as a function of time for different initial amplitudes  $A$  with same energy density. One observes an exponential decay of the anisotropy with  $\Delta F \rightarrow 0$  at late times. While the behavior at early times is sensitive to the initial amplitude, the isotropization rates become universal at late times. On the right the corresponding pressure differences normalized to the energy density are shown.

## 5 Numerical results

In the following we present the numerical solutions of the full equations (2.15) with the self-energies (2.20). The results are then confronted with the estimates from the relaxation-time approximation discussed above. We employ a rather weak coupling  $g^2 \equiv \lambda/4! = 1/4$  and consider a wide range of anisotropic initial conditions (2.12)–(2.13) with amplitudes  $A = 10 - 160$ . The width  $\sigma$  of the initial particle number distribution  $n_0(\vec{p})$  of Eq. (2.13) is chosen such that the energy expectation value is the same for the different initial conditions. Therefore, if the system thermalizes then the late-time results are determined by the same temperature. The employed energy density corresponds to that of a thermal system with temperature  $T = 1.03 m_R$ , where we always express dimensionful quantities in units of the renormalized thermal mass  $m_R$ .

We first consider the anisotropy correlator  $\Delta F(t_1, t_2; p_{ts})$  defined in Eq. (2.16) with  $p_{ts} = 0.93 m_R$ . At equal times  $t_1 = t_2$  it corresponds to the frequency integral of the corresponding correlator in Wigner space, i.e.  $\Delta F(t, t; p_{ts}) = \int [d\omega/2\pi] \Delta F(t; \omega, p_{ts})$  (cf. Sec. 3). The left graph of Fig. 5 shows the time evolution of  $\Delta F(t, t; p_{ts})$  normalized to  $2F(t, t; p_{ts})$

for different anisotropy amplitudes  $A$ . One observes that at early times the behavior of  $\Delta F/2F$  depends on the initial amplitude. However, for times  $t \gtrsim 300/m_R$  the isotropization rate becomes independent of the details of the initial conditions. It approaches an exponential behavior with rate  $\gamma_{\text{iso}}(p_{\text{ts}}) = 0.0061(2) m_R$ .

A similar behavior can be seen in the right graph of Fig. 5 for the pressure anisotropy  $\Delta P(t)$  normalized to the energy density  $\varepsilon$ . Its late-time isotropization rate turns out to be rather accurately described by the characteristic rate of the maximally populated mode, i.e.  $\gamma_{\text{iso}}(p_{\text{ts}})$ . The pressure anisotropy and energy density have been calculated from the diagonal components of the energy-momentum tensor (2.21) as  $\varepsilon \equiv T^{00}$  and  $\Delta P \equiv T^{33} - T^{11} \equiv T^{33} - T^{22}$ . A value reasonable for the use of hydrodynamics, say  $\Delta P/\varepsilon \lesssim 0.1$ , is reached particularly fast for large  $A$ .

In order to directly compare the results to the relaxation-time approximation (4.7), we consider the late-time evolution of the Wigner-space correlator  $\Delta F(t; \omega, p_{\text{ts}})$ . Following the results of Sec. 3,  $\Delta F(t; \omega, p_{\text{ts}})$  is described by the evolution equation (3.3) for sufficiently late times. If the relaxation-time approximation is valid then Eq. (3.3) can be replaced by the simpler expression of Eq. (4.5). Comparing the two equations one observes that in this case the ratio  $-(\bar{\Sigma}_\varrho \Delta F + \Delta \Sigma_\varrho \bar{F} - \bar{\Sigma}_F \Delta \varrho - \Delta \Sigma_F \bar{\varrho})/2\omega \Delta F$  must approach the relaxation-time rate  $\Sigma_\varrho^{(\text{eq})}/2\omega^{(\text{eq})}$ . To establish the equivalence, we first evaluate the former expression using the full solution of the nonequilibrium evolution from Eqs. (2.15) and (2.20). In a second calculation, we evaluate  $\Sigma_\varrho^{(\text{eq})}/2\omega^{(\text{eq})}$  directly in thermal equilibrium for the same energy density. The results of these calculations are shown in Fig. 1 for on-shell  $\omega$ , i.e. evaluated from the peak of the spectral function [11] for momentum  $p_{\text{ts}}$ . The lower curve of Fig. 1 shows the nonequilibrium time evolution of the ratio  $-(\bar{\Sigma}_\varrho \Delta F + \Delta \Sigma_\varrho \bar{F} - \bar{\Sigma}_F \Delta \varrho - \Delta \Sigma_F \bar{\varrho})/2\omega \Delta F$ . One observes that indeed for times  $t \gtrsim 500/m_R$  the nonequilibrium ratio approaches closely  $-\Sigma_\varrho^{(\text{eq})}/2\omega^{(\text{eq})}$ , where the latter value is indicated by the square symbol on the right of the figure. This verifies standard relaxation-time approximations for the description of isotropization at sufficiently late times.

It should be stressed that this agreement of the nonequilibrium isotropization rate with the normalized imaginary part of the *equilibrium self energy*, i.e.  $-\Sigma_\varrho^{(\text{eq})}/2\omega^{(\text{eq})}$ , is very nontrivial for relatively early times  $t \gtrsim 500/m_R$ : The imaginary part of the *nonequilibrium self-energy* at that

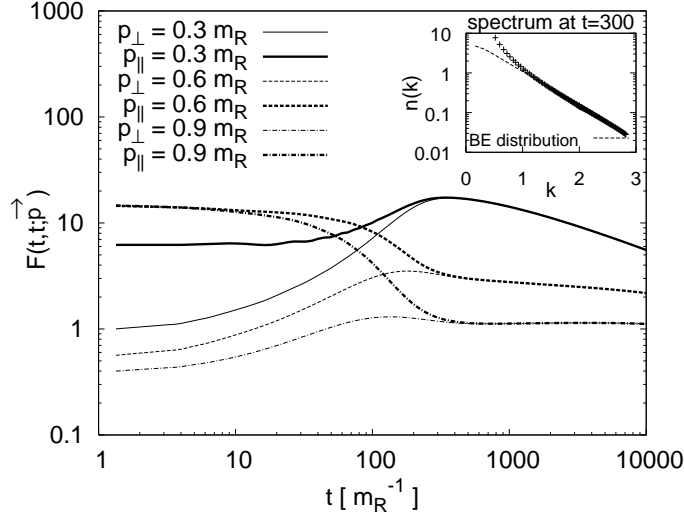


Figure 6: Equal-time correlator  $F(t, t; \vec{p}) \equiv F(t, t; p_\perp, p_\parallel)$  for different three-momenta as a function of time in units of the renormalized thermal mass  $m_R$ . The lines show the modes for transverse,  $F(t, t; p_\perp, 0)$ , and for longitudinal momenta,  $F(t, t; 0, p_\parallel)$ , for the values of  $p_\perp$  and  $p_\parallel$  as indicated in the figure. One observes isotropy with  $F(t, t; p_\perp, 0) = F(t, t; 0, p_\parallel)$  for  $p_\perp = p_\parallel$  to good accuracy for times  $t \gtrsim 300/m_R$ . In contrast, equilibrium has not been achieved at that time and the effectively isotropic modes continue to evolve towards a thermal distribution. For comparison, the dashed line of the inset shows the Bose-Einstein (BE) distribution along with the nonthermal time-dependent distribution function  $n(|\vec{k}|)$  as a function of  $|\vec{k}|/m_R$  at time  $t = 300/m_R$ .

time is still far from equilibrium! This is demonstrated in Fig. 1, where the upper curve shows the normalized imaginary part of the nonequilibrium self-energy, or  $-\bar{\Sigma}_\rho(t; \omega, \bar{q})/2\omega(t)$ . The calculation (solid line) was performed until  $t = 50000/m_R$ , and the dotted line in the figure represents a fit.<sup>9</sup> Only at very late times, i.e. much later than the inverse relaxation-time rate  $t \gg -2\omega^{(\text{eq})}/\Sigma_\rho^{(\text{eq})}$ , its nonequilibrium evolution comes rather close to its thermal value. This points out that the relaxation-time approximation fails to give an estimate for the thermalization time. According to the relaxation-

<sup>9</sup>The plotted fit is obtained using a power-law behavior, however, the available late-time range of numerical data can be fitted using an exponential behavior with comparable accuracy.

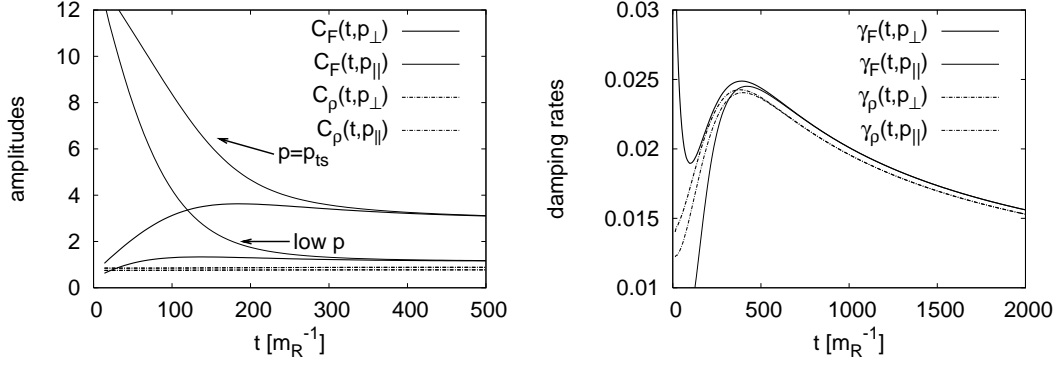


Figure 7: The left graph shows the evolution of the amplitudes and the right graph shows the damping rates extracted from the unequal-time correlators  $F$  and  $\rho$  as a function of  $t$ , as defined in Eq. (5.1) for the maximally amplified mode with  $|\vec{p}| = p_{ts}$  and for a low-momentum mode.

time approximation discussed in Sec. 4, the characteristic thermalization time agrees with the isotropization time  $-2\omega^{(eq)}/\Sigma_\rho^{(eq)}$ . This is sharp contrast with the findings represented in Fig. 1 showing a large separation of times between isotropization and thermalization. We emphasize that for the considered class of initial conditions the large separation is also found if the coupling is further weakened (cf. also the discussion in Sec. 4).

The faster isotropization as compared to thermalization can also be observed from the real-time correlator modes  $F(t, t; \vec{p})$  in Fig. 6. Isotropy implies  $F(t, t; p_\perp, 0) = F(t, t; 0, p_\parallel)$  for  $p_\perp = p_\parallel$ , which is achieved to good accuracy for times  $t \gtrsim 300/m_R$ . In contrast, the modes still show strong deviations from thermal equilibrium at that time. To emphasize this fact the inset compares the time-dependent nonthermal effective particle number distribution [37, 11, 14]  $n(\vec{k}) \simeq n(|\vec{k}|)$  as a function of  $|\vec{k}|/m_R$  at time  $t = 300/m_R$  with the Bose-Einstein distribution.

The amplitudes and damping rates plotted in Fig. 7 are the fit parameters  $C_{F/\rho}$  and  $\gamma_{F/\rho}(t; \vec{p})$ , respectively, in

$$\begin{aligned} F(t_1, t_2; \vec{p}) &= C_F(t; \vec{p}) \cos[\omega_F(t; \vec{p})(t_1 - t_2)] e^{-\gamma_F(t; \vec{p})(t_1 - t_2)} \\ \rho(t_1, t_2; \vec{p}) &= C_\rho(t; \vec{p}) \sin[\omega_\rho(t; \vec{p})(t_1 - t_2)] e^{-\gamma_\rho(t; \vec{p})(t_1 - t_2)} \end{aligned} \quad (5.1)$$

The values are extracted at each  $t = (t_1 + t_2)/2$  adjusting  $C_{F/\rho}(t; \vec{p})$ ,  $\omega_{F/\rho}(t; \vec{p})$  and  $\gamma_{F/\rho}(t; \vec{p})$ . We observe (not shown in the plot) an isotropic  $\omega_{F/\rho}(t; \vec{p})$  parameter from the very beginning. In thermal equilibrium the

damping parameters of Eq. (5.1) would equal half the rate  $-\Sigma_\rho(t;\omega)/2\omega$  if the correlator modes  $F(t;\omega,\vec{p})$  and  $\rho(t;\omega,\vec{p})$  were of exact Breit-Wigner form.

## 6 Conclusions

Isotropization happens much faster than the approach to thermal equilibrium. This is not a surprising fact, since only a subclass of those processes that lead to thermalization are actually required for isotropization: “ordinary”  $2 \leftrightarrow 2$  scattering processes are sufficient in order to isotropize a system, while global particle number changing processes are crucial to approach thermal equilibrium. For the massive weak-coupling scalar theory, the  $2 \leftrightarrow 2$  processes are of order  $\lambda^2$ , while global number changing processes such as  $1 \leftrightarrow 3$  processes are of order  $\lambda^4$ . For small couplings the  $2 \leftrightarrow 2$  scatterings can, therefore, dominate the early-time behavior. While these processes are in principle sufficient to achieve complete isotropization, they are not sufficient to provide a quantitative description of thermalization. In the absence of global particle number changing processes they would, for instance, lead to a spurious chemical potential in the Bose-Einstein distribution at late times, which is clearly absent for the thermal equilibrium theory of real scalar fields.

We demonstrate that these apparently small higher order contributions lead to quantitatively important corrections for general nonequilibrium situations. To establish this requires to go beyond the relaxation-time approximation, which fails to describe the dynamics close to equilibrium in general. We emphasize in Sec. 4 that the relaxation-time ansatz neglects, in particular, all off-diagonal elements in the stability matrix around thermal equilibrium. Whether the true small eigenvalues of the stability matrix play an important role for the late-time behavior depends on the physical quantity of interest. We have shown that the isotropization rate is at sufficiently late times well described by the relaxation-time approximation, though the latter fails even to give a correct order-of-magnitude estimate for the thermal equilibration time.

Since our approach does not involve a gradient expansion, we can determine the range of validity of a description to lowest-order in gradients, which is typically employed in kinetic equations and to motivate the relaxation-time ansatz close to equilibrium. The earliest time for the applicability of the lowest-order gradient expansion is found to be of the

order of the characteristic isotropization time  $\tau_{\text{iso}}$ .

Far-from-equilibrium isotropization can be very important for the understanding of collision experiments of heavy nuclei. An isotropic equation of state  $P/\varepsilon$  is a crucial ingredient for the apparently successful application of hydrodynamic descriptions. We have shown in a previous publication that the prethermalization [1] of the equation of state to its equilibrium value is insensitive to the thermal equilibration time  $\tau_{\text{eq}}$ . The relevant time scale for the early validity of hydrodynamics could then be set by the isotropization time, which can be much shorter than  $\tau_{\text{eq}}$ . In this context it is interesting to note that our simple scalar theory indicates that large initial anisotropies can lead to enhanced characteristic isotropization rates as compared to conventional relaxation-time rates.

## References

- [1] J. Berges, S. Borsanyi and C. Wetterich, “Prethermalization,” Phys. Rev. Lett. **93** (2004) 142002 [arXiv:hep-ph/0403234].
- [2] U. W. Heinz, “Thermalization at RHIC,” AIP Conf. Proc. **739** (2005) 163 [arXiv:nucl-th/0407067].
- [3] P. Arnold, J. Lenaghan, G. D. Moore and L. G. Yaffe, “Apparent thermalization due to plasma instabilities in quark gluon plasma,” Phys. Rev. Lett. **94** (2005) 072302 [arXiv:nucl-th/0409068].
- [4] S. Mrowczynski, “Plasma instability at the initial stage of ultrarelativistic heavy ion collisions,” Phys. Lett. B **314** (1993) 118; “Color collective effects at the early stage of ultrarelativistic heavy ion collisions,” Phys. Rev. C **49** (1994) 2191; “Color filamentation in ultrarelativistic heavy-ion collisions,” Phys. Lett. B **393** (1997) 26 [arXiv:hep-ph/9606442];
- [5] P. Romatschke and M. Strickland, “Collective modes of an anisotropic quark gluon plasma,” Phys. Rev. D **68** (2003) 036004 [arXiv:hep-ph/0304092]. A. Rebhan, P. Romatschke and M. Strickland, “Hard-loop dynamics of non-Abelian plasma instabilities,” Phys. Rev. Lett. **94** (2005) 102303 [arXiv:hep-ph/0412016].



- [6] E. V. Shuryak and I. Zahed, “Rethinking the properties of the quark gluon plasma at  $T \approx T(c)$ ,” *Phys. Rev. C* **70** (2004) 021901 [arXiv:hep-ph/0307267]. Z. Xu and C. Greiner, “Thermalization of gluons in ultrarelativistic heavy ion collisions by including three-body interactions in a parton cascade,” arXiv:hep-ph/0406278. F. Gastineau, E. Blanquier and J. Aichelin, “Critical opacity: A possible explanation of the fast thermalisation times seen in RHIC experiments,” arXiv:hep-ph/0404207.
- [7] For a review see J. Berges, “Introduction to nonequilibrium quantum field theory,” *AIP Conf. Proc.* **739** (2005) 3 [arXiv:hep-ph/0409233]. J. Berges and J. Serreau, “Progress in nonequilibrium quantum field theory,” in *SEWM02*, ed. M.G. Schmidt (World Scientific, 2003) [arXiv:hep-ph/0302210]; *SEWM04*, eds. K.J. Eskola, K. Kainulainen, K. Kajantie and K. Rummukainen (World Scientific, 2005) [arXiv:hep-ph/0410330].
- [8] H. A. Weldon, “Simple Rules For Discontinuities In Finite Temperature Field Theory,” *Phys. Rev. D* **28** (1983) 2007. this see e.g. L. Kadanoff and G. Baym, “Quantum Statistical Mechanics,” Benjamin, New York, 1962.
- [9] D. Boyanovsky, I. D. Lawrie and D. S. Lee, “Relaxation and Kinetics in Scalar Field Theories,” *Phys. Rev. D* **54** (1996) 4013 [arXiv:hep-ph/9603217].
- [10] J. Berges and J. Cox, “Thermalization of quantum fields from time-reversal invariant evolution equations,” *Phys. Lett. B* **517** (2001) 369 [arXiv:hep-ph/0006160]. J. Berges, “Controlled nonperturbative dynamics of quantum fields out of equilibrium,” *Nucl. Phys. A* **699** (2002) 847 [arXiv:hep-ph/0105311].
- [11] G. Aarts and J. Berges, “Nonequilibrium time evolution of the spectral function in quantum field theory,” *Phys. Rev. D* **64** (2001) 105010 [arXiv:hep-ph/0103049].
- [12] F. Cooper, J. F. Dawson and B. Mihaila, “Quantum dynamics of phase transitions in broken symmetry  $\lambda\phi^4$  field theory,” *Phys. Rev. D* **67** (2003) 056003 [arXiv:hep-ph/0209051]. B. Mihaila, F. Cooper and J. F. Dawson, “Resumming the large- $N$  approximation

- for time evolving quantum systems,” Phys. Rev. D **63** (2001) 096003 [arXiv:hep-ph/0006254].
- [13] J. Berges and J. Serreau, “Parametric resonance in quantum field theory,” Phys. Rev. Lett. **91** (2003) 111601 [arXiv:hep-ph/0208070].  
G. Aarts, D. Ahrensmeier, R. Baier, J. Berges and J. Serreau, “Far-from-equilibrium dynamics with broken symmetries from the 2PI-1/N expansion,” Phys. Rev. D **66** (2002) 045008 [arXiv:hep-ph/0201308].
  - [14] J. Berges, S. Borsanyi and J. Serreau, “Thermalization of fermionic quantum fields,” Nucl. Phys. B **660** (2003) 51 [arXiv:hep-ph/0212404].
  - [15] S. Juchem, W. Cassing and C. Greiner, “Quantum dynamics and thermalization for out-of-equilibrium  $\phi^4$ -theory,” Phys. Rev. D **69** (2004) 025006 [arXiv:hep-ph/0307353].
  - [16] D. J. Bedingham, “Out-of-equilibrium quantum fields with conserved charge,” Phys. Rev. D **69** (2004) 105013 [arXiv:hep-ph/0310133].
  - [17] A. Arrizabalaga, J. Smit and A. Tranberg, “Equilibration in  $\phi^4$  theory in 3+1 dimensions,” arXiv:hep-ph/0503287. “Tachyonic preheating using 2PI - 1/N dynamics and the classical approximation,” JHEP **0410** (2004) 017 [arXiv:hep-ph/0409177].
  - [18] J. M. Cornwall, R. Jackiw and E. Tomboulis, “Effective Action For Composite Operators,” Phys. Rev. D **10** (1974) 2428; see also J. M. Luttinger and J. C. Ward, Phys. Rev. **118** (1960) 1417; G. Baym, Phys. Rev. **127** (1962) 1391.
  - [19] H. van Hees and J. Knoll, “Renormalization in self-consistent approximations schemes at finite temperature. I: Theory,” Phys. Rev. D **65** (2002) 025010 [arXiv:hep-ph/0107200]. H. Van Hees and J. Knoll, “Renormalization of self-consistent approximation schemes. II: Applications to the sunset diagram,” Phys. Rev. D **65** (2002) 105005 [arXiv:hep-ph/0111193].
  - [20] S. Borsanyi and Z. Szep, “Relaxation of 2+1 dimensional classical O(2) symmetric scalar fields,” Phys. Lett. B **508** (2001) 109 [arXiv:hep-ph/0011283].

- [21] J. Berges, S. Borsanyi, U. Reinosa and J. Serreau, “Nonperturbative renormalization for 2PI effective action techniques,” arXiv:hep-ph/0503240. “Renormalized thermodynamics from the 2PI effective action,” Phys. Rev. D **71** (2005) 105004 [arXiv:hep-ph/0409123].
- [22] J. P. Blaizot, E. Iancu and U. Reinosa, “Renormalizability of  $\Phi$ -derivable approximations in scalar  $\phi^4$  theory,” Phys. Lett. B **568** (2003) 160 [arXiv:hep-ph/0301201]. “Renormalization of  $\phi$ -derivable approximations in scalar field theories,” Nucl. Phys. A **736** (2004) 149 [arXiv:hep-ph/0312085].
- [23] F. Cooper, B. Mihaila and J. F. Dawson, “Renormalizing the Schwinger-Dyson equations in the auxiliary field formulation of  $\lambda \phi^4$  field theory,” Phys. Rev. D **70** (2004) 105008 [arXiv:hep-ph/0407119]. F. Cooper, J. F. Dawson and B. Mihaila, “Renormalized broken-symmetry Schwinger-Dyson equations and the 2PI-1/N expansion for the  $O(N)$  model,” arXiv:hep-ph/0502040.
- [24] J. Berges and M. M. Muller, “Nonequilibrium quantum fields with large fluctuations,” in Progress in Nonequilibrium Green’s Functions II, eds. M. Bonitz and D. Semkat, World Scientific (2003) [<http://arXiv:hep-ph/0209026>].
- [25] J. Berges, “n-Particle irreducible effective action techniques for gauge theories,” Phys. Rev. D **70** (2004) 105010 [arXiv:hep-ph/0401172].
- [26] L. Kadanoff and G. Baym, “Quantum Statistical Mechanics”, Benjamin, New York, 1962.
- [27] P. Danielewicz, “Quantum Theory Of Nonequilibrium Processes. I,” Annals Phys. **152** (1984) 239. S. Mrowczynski and P. Danielewicz, “Green Function Approach To Transport Theory Of Scalar Fields,” Nucl. Phys. B **342**, 345 (1990).
- [28] K. c. Chou, Z. b. Su, B. l. Hao and L. Yu, “Equilibrium And Nonequilibrium Formalisms Made Unified,” Phys. Rept. **118**, 1 (1985).
- [29] E. Calzetta and B. L. Hu, “Nonequilibrium Quantum Fields: Closed Time Path Effective Action, Wigner Function And Boltzmann Equation,” Phys. Rev. D **37**, 2878 (1988).

- [30] C. Greiner and S. Leupold, “Stochastic interpretation of Kadanoff-Baym equations and their relation to Langevin processes,” *Annals Phys.* **270**, 328 (1998) [arXiv:hep-ph/9802312].
- [31] Y. B. Ivanov, J. Knoll and D. N. Voskresensky, *Nucl. Phys. A* **657** (1999) 413 [arXiv:hep-ph/9807351].
- [32] J. P. Blaizot and E. Iancu, “The quark-gluon plasma: Collective dynamics and hard thermal loops,” *Phys. Rept.* **359**, 355 (2002) [arXiv:hep-ph/0101103].
- [33] P. Lipavsky, K. Morawetz and V. Spicka, “Kinetic equation for strongly interacting dense Fermi systems,” *Annales de Physique*, Vol. 26, No. 1 (2001) 1.
- [34] T. Prokopec, M. G. Schmidt and S. Weinstock, “Transport equations for chiral fermions to order  $\hbar$  and electroweak baryogenesis,” *Annals Phys.* **314** (2004) 208 [arXiv:hep-ph/0312110]. *Annals Phys.* **314** (2004) 267 [arXiv:hep-ph/0406140]. T. Konstandin, T. Prokopec, M. G. Schmidt and M. Seco, “MSSM Electroweak Baryogenesis and Flavour Mixing in Transport Equations,” arXiv:hep-ph/0505103.
- [35] A. Jakovac, “Time evolution in linear response: Boltzmann equations and beyond,” *Phys. Rev. D* **65** (2002) 085029 [arXiv:hep-ph/0112188].
- [36] S. Jeon, “Computing spectral densities in finite temperature field theory,” *Phys. Rev. D* **47** (1993) 4586. E.-k. Wang and U. W. Heinz, “The plasmon in hot  $\phi^4$  theory,” *Phys. Rev. D* **53** (1996) 899.
- [37] M. Salle, J. Smit and J. C. Vink, “Thermalization in a Hartree ensemble approximation to quantum field dynamics,” *Phys. Rev. D* **64** (2001) 025016 [arXiv:hep-ph/0012346].